Understanding the Highly Regioselective Cyanothiolation of 1-Alkynes Catalyzed by Palladium Phosphine Complexes

Wenxu Zheng,[†] Alireza Ariafard,*[,‡] and Zhenyang Lin*[,†]

Department of Chemistry, The Hong Kong University of Science and Technology, Clear Water Bay, Kowloon, Hong Kong, and Department of Chemistry, Faculty of Science, Central Tehran Branch, Islamic Azad University, Felestin Square, Tehran, Iran

Received September 21, 2007

A computational study with the Becke3LYP DFT functional was carried out on the palladium-catalyzed regioselective cyanothiolation of 1-alkynes with thiocyanates. The full catalytic cycle was computed, starting from the oxidative addition and finishing with the reductive elimination. The two most important issues, namely, the regioselective bond cleavage of thiocyanates and the nature of insertion of 1-alkynes into a Pd−S bond, are discussed. The calculations indicate that the sulfur−cyano (PhS−CN) bond cleavage on Pd(0) is kinetically and thermodynamiclly more favorable than the carbon−sulfur (Ph−SCN) bond cleavage. The kinetic preference of 1,2-insertion over 2,1-insertion in the alkyne insertion step leads to the cyanothiolation products with the SPh group attached to the substituted carbon atom of 1-alkynes.

Introduction

Many organic heteroatom compounds such as organosilicon, organoboron, and organotin are very useful species in transition-metal-catalyzed carbon−carbon bond formations.[1] However, group 16 heteroatom compounds used to be recognized as catalyst poisons in the transition-metal-catalyzed reactions, leading to the rare appearance of these compounds in the catalyzed reactions.[2] In 1991, Ogawa et al. first showed an efficient transition-metal-catalyzed addition of organic disulfides to alkynes.[3] Since then, organosulfur compounds have attracted attention in transition-metal-catalyzed reactions, and several synthetically useful transition-metal-catalyzed addition reactions of organosulfur compounds to unsaturated compounds have been developed by many groups.[4,5] Recently, Ogawa et al. reported a highly regioselective cyanothiolation of alkynes catalyzed by tetrakis(triphenylphosphine)palladium(0) eq 1. The reactions introduce both thio and cyano groups into the internal and terminal positions of 1-alkynes, respectively, with excellent regioselectivity. In addition, the cyanothiolation reactions mainly produce products having a *Z*-configuration about the double bond. It was proposed that the reactions proceeded via a mechanism similar to many other Pd-catalyzed cross-coupling reactions, which starts with an oxidative addition of thiocyanates followed by a thiopalladation or a cyanopalladation and then a reductive elimination.

In the alkyne cyanothiolation reactions reported by Ogawa et al., there are two interesting and important issues that require theoretical studies. The first one concerns the bond cleavage in thiocyanates. It was found that the oxidative addition of PhSCN to Pd(0) proceeds with the cleavage of the PhS−CN bond rather than the Ph−SCN bond. It has been known that the bond cleavage in thiocyanates can occur at either the α (R−SCN) or β (RS−CN) bond. Houmam et al. investigated the electrochemical reduction of a series of substituted phenyl and benzyl thiocyanates.[7] For the phenyl thiocyanates, only the β bond cleavage can be observed, but for the benzyl thiocyanates, both the α and β bonds can be cleaved, depending on the substituents on the benzyl ring.

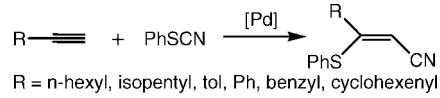

(1)

Another important issue that needed to be addressed is the regioselectivity of the cyanothiolation of the terminal alkynes. In the experiments, the thio group is always introduced to the internal position of the alkynes.[6] It is unclear what factors determine the regioselectivity.

In this work, we investigated the mechanism of the Pd-catalyzed cyanothiolation of 1-alkynes in detail and addressed the two important issues mentioned above.

* Corresponding author. E-mail: ariafard@yahoo.com, chzlin@ust.hk.
[†] The Hong Kong University of Science and Technology.
[‡] Islamic Azad University.

(1) (a) Ojima, I. In *The Chemistry Organic Silicon Compounds*; Patai, S., Rappopot, Z., Eds.; Wiley-Interscience: Chichester, 1989. (b) Davies, A. G. *Organotin Chemistry*; VCH: Weinheim, 1997. (c) Orita, A.; Otera, J. In *Main Group Metals in Organic Synthesis*; Yamamoto, H. , Oshima, K., Eds.; Wiley-VCH: Weinheim, 2004; Vol. *2*,Chapter 12.

(2) Hegedus, L. L.; McCabe, R. W. *Catalyst Poisoning*; Marcel Dekker: New York, 1984.

(3) Kuniyasu, H.; Ogawa, A.; Miyazaki, S.; Ryu, I.; Kambe, N.; Sonoda, N. *J. Am. Chem. Soc.* **1991**, *113*, 9796.

(4) (a) Ogawa, A. In *Handbook of Organopalladium Chemistry for Organic Synthesis*; Negishi, E., Ed.; Wiley: New York, 2002;Chapter VII.6. (b) Alonso, F.; Beletskaya, I. P.; Yus, M. *Chem. Rev.* **2004**, *104*, 3079. (c) Ogawa, A. In *Main Group Metals in Organic Synthesis*; Yamamoto, H., Oshima, K., Eds.; Wiley-VCH: Weinheim, 2004; Vol. 2,Chapter 15.

(5) (a) Kuniyasu, H.; Ogawa, A.; Miyazaki, S.; Ryu, I.; Kambe, N.; Sonoda, N. *J. Am. Chem. Soc.* **1991**, *113*, 9796. (b) Kuniyasu, H.; Ogawa, A.; Sato, K.; Ryu, I.; Kambe, N.; Sonoda, N. *J. Am. Chem. Soc.* **1992**, *114*, 5902. (c) Ogawa, A.; Takeba, M.; Kawakami, J.; Ryu, I.; Kambe, N.; Sonoda, N. *J. Am. Chem. Soc.* **1995**, *117*, 7564. (d) Ogawa, A.; Kawakami, J.; Mihara, M.; Ikeda, T.; Sonoda, N.; Hirao, T. *J. Am. Chem. Soc.* **1997**, *119*, 12380. (e) Ogawa, A.; Kawakami, J.; Sonoda, N.; Hirao, T. *J. Org. Chem.* **1996**, *61*, 4161. (f) Ogawa, A.; Ikeda, T.; Kimura, K.; Hirao, T. *J. Am. Chem. Soc.* **1999**, *121*, 5108. (g) Ogawa, A. *J. Organomet. Chem.* **2000**, *611*, 463. (h) Kawakami, J.; Takeba, M.; Kamiya, I.; Sonoda, N.; Ogawa, A. *Tetrahedron* **2003**, *59*, 6559.

(6) Kamiya, I.; Kawakami, J.; Yano, S.; Nomoto, A.; Ogawa, A. *Organometallics* **2006**, *25*, 3562.

(7) Hamed, E. M.; Doai, H.; McLaughlin, C. K.; Houmam, A. *J. Am. Chem. Soc.* **2006**, *128*, 6595.

10.1021/om7009446 CCC: $40.75
Publication on Web 12/27/2007

Scheme 1

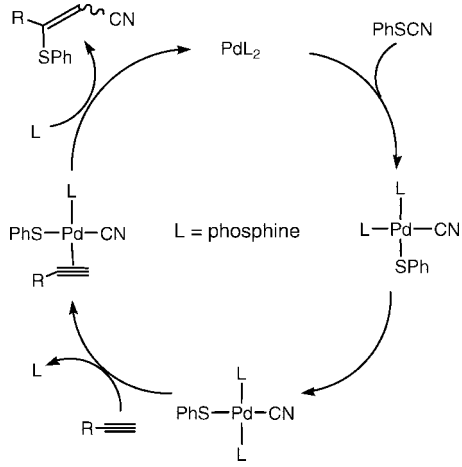

Computational Details

Molecular geometries of the complexes were optimized at the Becke3LYP level of density functional theory.[8] Frequency calculations at the same level of theory were also performed to identify all the stationary points as minima (zero imaginary frequencies) or transition states (one imaginary frequency) and to provide free energies at 298.15 K. The intrinsic reaction coordinate (IRC)[9] analysis was carried out to confirm that all stationary points are smoothly connected to each other. The Pd, S, and P atoms were described using the LANL2DZ basis set including a double-ζ valence basis set with the Hay and Wadt effective core potential (ECP).[10] An additional d polarization shell was added for S and P with exponents of 0.421 and 0.340, respectively.[11] The 6-31G[12] basis set was used for other atoms, and polarization functions were added for C ($\zeta_d = 0.600$) and N ($\zeta_d = 0.864$).[11] Molecular orbitals obtained from the B3LYP calculations were plotted using the Molden 3.7 program written by Schaftenaar.[13] All calculations were performed with Gaussian 03 packages.[14] In most of our DFT calculations, we used PH_3 as a model for PPh_3. To study the steric effect missed from the small model calculations, we performed two-layer ONIOM[15] (B3LYP/BSI:HF/Lanl2MB) calculations with the real PPh_3 ligand for several selected species. In the ONIOM calculations, the phenyl groups attached to phosphorus atoms were treated at the lower level method, HF with the Lanl2MB minimal basis set,[10] while the rest were treated at the higher level method, B3LYP with the same basis set as those in the model calculations (BSI).

Results and Discussion

A. Oxidative Addition of Thiocyanatobenzene to Palladium(0). Scheme 1 shows the proposed reaction mechanism for the catalytic cyanothiolation of alkynes. Similar to many other Pd-catalyzed cross-coupling reactions, the first step involves oxidative addition of electrophiles to the coordinatively unsaturated 14-electron species "$L_2Pd(0)$". Ogawa et al. have isolated the square-planar complex *trans*-$Pd(SPh)(CN)(PPh_3)_2$ by reacting $Pd(PPh_3)_4$ with 1 equiv of PhSCN.[6] The square-planar complex can also catalyze the cyanothiolation reactions. The oxidative addition of PhSCN proceeds with the cleavage of the sulfur−cyano bond (PhS−CN), not the carbon−sulfur bond (Ph−SCN). As mentioned in the Introduction, the bond cleavage in the RSCN compounds could occur at either the α (R−SCN) bond or the β (RS−CN) bond. We first calculated the bond dissociation energies for both the α and β bonds for the PhSCN molecule. The results show a large difference between the α and β bond strengths, with the β bond being about 15 kcal/mol stronger than the α one. The β bond dissociation energy (PhSCN → PhS + CN) was calculated to be 89 kcal/mol, while the α bond dissociation energy (PhSCN → Ph + SCN) was calculated to be 74 kcal/mol. The difference in the bond dissociation energies is expected, as it is generally believed that the α bond cleavage is more facile than the β one. Interestingly, the oxidative addition observed in the alkyne cyanothiolation reactions reported by Ogawa et al. cleaves the stronger bond rather than the weaker one.

The calculated potential energy profiles for the oxidative addition of PhSCN to $Pd(PPh_3)_2$ illustrated in Figure 1 show a kinetically and thermodynamically favorable β cleavage, consistent with the experimental findings. In the figure, the relative free energies (ΔG) and electronic energies (ΔE, in parentheses) are given for model

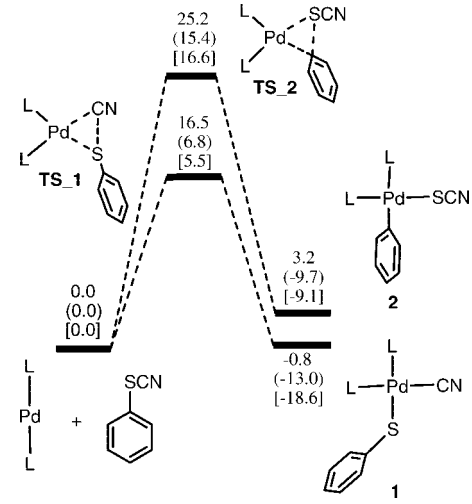

Figure 1. Potential energy profiles calculated for the oxidative addition of PhSCN to $Pd(PPh_3)_2$. The relative free energies (kcal/mol) and electronic energies (kcal/mol, in parentheses) are given for model systems ($L = PH_3$). The relative electronic energies (kcal/mol) in brackets were obtained on the basis of the ONIOM calculations, which consider the steric effect of the realistic PPh_3 ligands.

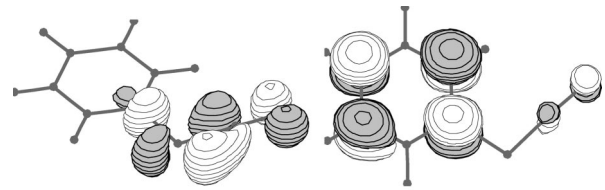

Figure 2. Spatial plots and the orbital energies of the LUMO (left) and LUMO+1 (right) for PhSCN.

(8) (a) Becke, A. D. *J. Chem. Phys.* **1993**, *98*, 5648. (b) Lee, C.; Yang, W.; Parr, R. G. *Phys. Rev. B* **1988**, *37*, 785. (c) Stephens, P. J.; Devlin, F. J.; Chabalowski, C. F.; Frisch, M. J. *J. Phys. Chem.* **1994**, *98*, 11623.

(9) (a) Fukui, K. *J. Phys. Chem.* **1970**, *74*, 4161. (b) Fukui, K. *Acc. Chem. Res.* **1981**, *14*, 363.

(10) (a) Hay, P. J.; Wadt, W. R. *J. Chem. Phys.* **1985**, *82*, 299. (b) Wadt, W. R.; Hay, P. J. *J. Chem. Phys.* **1985**, *82*, 284.

(11) Huzinaga, S. *Gaussian Basis Sets for Molecular Calculations*; Elsevier Science Pub. Co.: Amsterdam, 1984.

(12) Hariharan, P. C.; Pople, J. A. *Theor. Chim. Acta* **1973**, *28*, 213.

(13) Schaftenaar, G. *Molden v3.7*; CAOS/CAMM Center Nijmegen: Toernooiveld, Nijmegen, The Netherlands, 2001.

(14) Pople J. A.; et al. *Gaussian 03, Revision B.05*; Gaussian, Inc.: Pittsburgh, PA, 2003.

(15) (a) For references to the ONIOM method, see: Dapprich, S.; Komáaromi, I.; Byun, K. S.; Morokuma, K.; Frisch, M. J. *J. Mol. Struct. (THEOCHEM)* **1999**, *462*, 1. (b) Vreven, T.; Morokuma, K. *J. Comput. Chem.* **2000**, *21*, 1419. For a similar two-layer ONIOM calculation, see:. (c) Ananikov, V. P.; Szilagyi, R.; Morokuma, K.; Musaev, D. G. *Organometallics* **2005**, *24*, 1938.

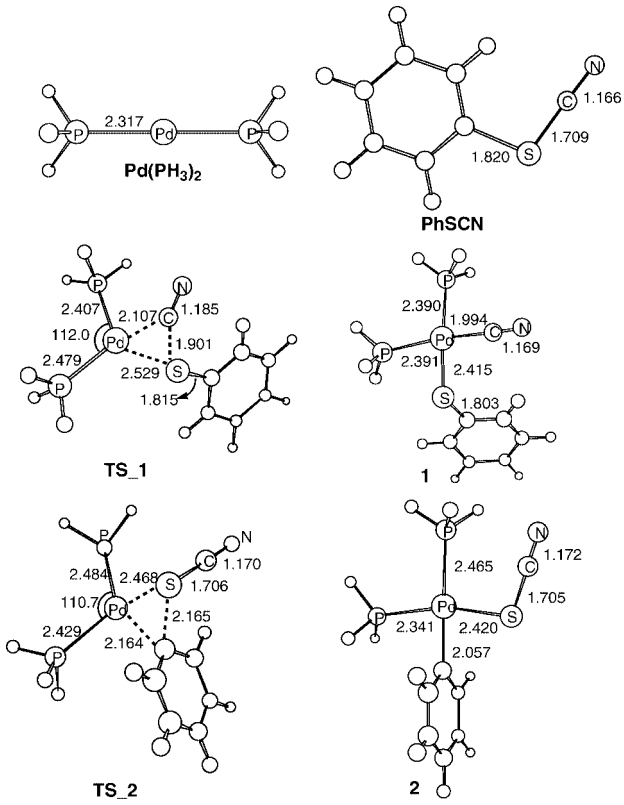

Figure 3. Selected structural parameters (Å) calculated for the species shown in Figure 1.

systems (L = PH_3). To examine the reliability of the PH_3 model systems, we also performed two-layer ONIOM calculations with the PPh_3 ligands. The relative electronic energies are given in brackets in Figure 1. From the figure, we can see that all the PH_3 model systems and their corresponding PPh_3 systems have similar relative electronic energies ΔE except the oxidative addition product **1**. The difference in the relative electronic energies between the PH_3 and PPh_3 systems for **1** is calculated to be 5.6 kcal/mol, much greater than expected. We do not have an explanation for this discrepancy. To further check if the PH_3 model calculations give reliable results, we extended the ONIOM calculations with the PPh_3 ligands to the species **4**, **TS_5**, and **TS_6**, which were important in the regioselectivity discussed below. The PPh_3-ONIOM calculations give relative electronic energies of −10.1 kcal/mol for **4**, −2.3 kcal/mol for **TS_5** and 1.7 kcal/mol for **TS_6**. The corresponding PH_3 model calculations give relative electronic energies of −12.0 kcal/mol for **4**, −4.6 kcal/mol for **TS_5**, and −0.9 kcal/mol for **TS_6**. These results indicate that the PH_3 model systems can describe the reactions properly. These results are understandable because the systems dealt with here have small coordination numbers and the steric effect of the bulky PPh_3 is relatively less important. Our discussion below will focus on the PH_3 model systems. Taking into account the effect of entropy, we use the free energies rather than the electronic energies (without ZPE correction) for our discussion since the reactions studied here involve two or more molecules.

The energy profiles reveal that the β bond cleavage of PhSCN on the Pd(0) center needs to overcome an energy barrier of only 16.5 kcal/mol, which is much lower than the corresponding energy barrier of 25.2 kcal/mol for the α bond cleavage. Moreover, examining the oxidative products, it is seen that **1**, generated from the β bond cleavage, is energetically located at 4.0 kcal/mol below **2**, derived from the α bond cleavage. These

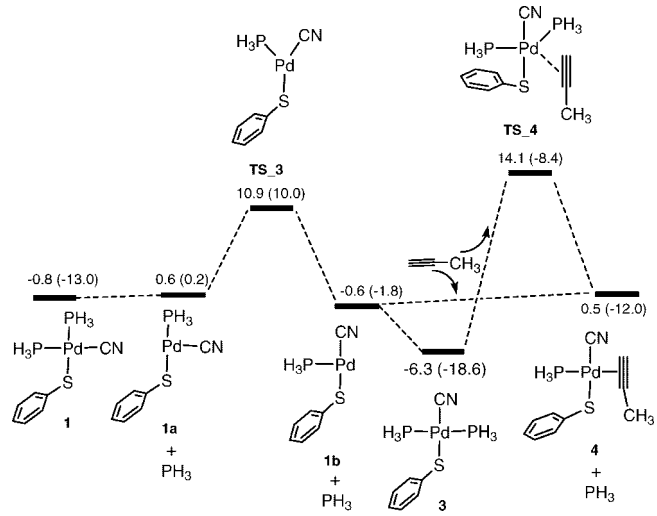

Figure 4. Potential energy profiles calculated for the *cis*-to-*trans* isomerization and substitution of PH_3 with a propyne substrate molecule in the square-planar complex $Pd(SPh)(CN)(PH_3)_2$. The relative free energies and electronic energies (in parentheses) are given in kcal/mol.

results indicate clearly that the β bond cleavage of PhSCN is much more favorable than the α bond cleavage both kinetically and thermodynamically, although the β bond is stronger than the α one.

Oxidative addition involves breaking of a C−S bond. Electron transfer occurs from the Pd(0) metal center to the substrate molecule. Therefore, we expect that the different reactivity of the two different C−S bonds in PhSCN is likely related to the characteristics of the LUMO of PhSCN, which acts as an acceptor of electrons during the oxidative addition process, similar to what we found in oxidative addition of aryl halides to Pd(0).[16] Figure 2 shows the spatial plots of the LUMO. We can easily find that the LUMO corresponds mainly to a π*-antibonding orbital in the SCN moiety. When the PhSCN substrate approaches the $Pd(PPh_3)_2$ fragment, the electrons back-donated by the Pd center are easily hosted by the π* orbital of the SCN moiety, facilitating the β bond cleavage. On the contrary, the electron transfer to the phenyl moiety leading to the α bond cleavage is relatively harder because the virtual orbitals having Ph−SCN π*-antibonding character are lying much higher. The easier electron transfer to the SCN moiety makes **TS_1** an early transition state. In contrast, **TS_2** is a late transition state, which is confirmed by the calculated structures of the transition states shown in Figure 3. The S−CN bond is stretched by 0.192 Å in **TS_1**, while the Ph−SCN bond is stretched by 0.345 Å in **TS_2**, indicating that **TS_1** is an earlier transition state than **TS_2**. For the oxidative products, **1** has shorter Pd−S and Pd−C bonds than **2**. Moreover, the phenyl ligand shows a larger *trans* influence in comparison with the cyano ligand since the Pd−P bond *trans* to CN in **1** is 0.08 Å shorter than the one *trans* to Ph in **2**. These structural parameters reveal that **1** possesses better Pd−ligand interactions, being thermodynamically more stable than **2**. Deviation of the metal–ligand geometric parameters of the PH_3 model systems shown in Figure 3 from those of the PPh_3 systems illustrated in Figure S1 in the Supporting Information is small, indicating again that the model systems are appropriate for our study here.

B. *cis*-to-*trans* Isomerization and Ligand Substitution of *trans*-$Pd(SPh)(CN)(PH_3)_2$. As mentioned above, PhSCN reacts with $Pd(PH_3)_2$ through a three-centered transition state, giving rise to the *cis*-$Pd(SPh)(CN)(PH_3)_2$ complex **1**. Experimentally, it

(16) Ariafard, A.; Lin, Z. *Organometallics* **2006**, *25*, 4030.

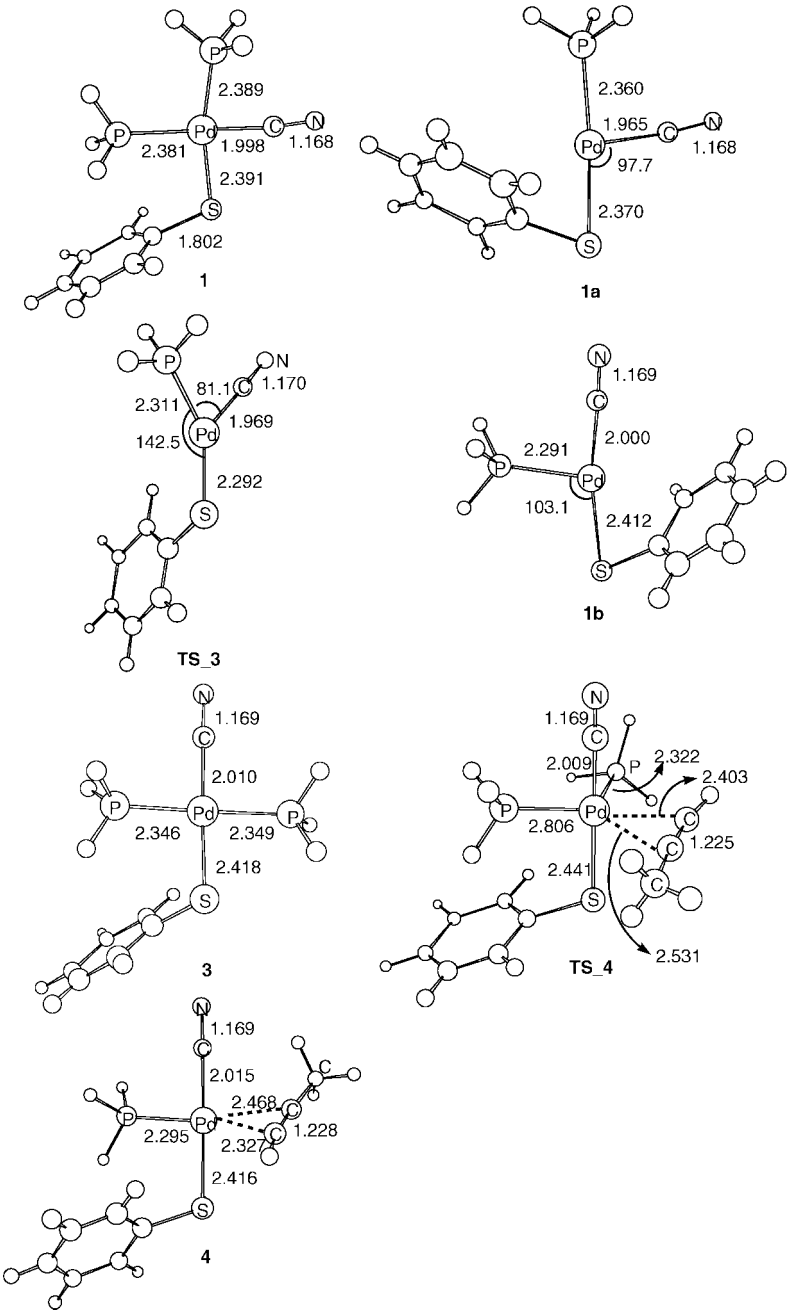

Figure 5. Selected structural parameters (Å) calculated for the species shown in Figure 4.

was found that the *cis*-isomer would subsequently isomerize to the thermodynamically more stable *trans*-isomer.[6] An analogous *cis*-to-*trans* isomerization process in the square-planar complex $(H_2C{=}CH)PdBr(PH_3)_2$ was reported by Maseras and co-workers.[17] They observed that the direct *cis*/*trans* four-coordinate rearrangement has quite a high barrier, while the other two alternative mechanisms, involving either phosphine dissociation or association of an external ligand, have a significantly lower energy barrier. On the basis of their work, we can safely assume that regardless of which mechanism the isomerization undergoes, this step should not be a critical obstacle for the overall process. Therefore, we discuss here only the isomerization process involving a three-coordinate rearrangement, with an initial loss of a phosphine ligand, passing through the intermediates **1a** and **1b**. The energy profile for the whole *cis*-to-*trans* isomerization is summarized in Figure 4. The monophosphine intermediate **1a** can be obtained by dissociating the phosphine *trans* to cyano in the *cis* square-planar complex **1**, and the intermediate **1b** can produce the *trans* square-planar complex **3** by simply coordinating with a phosphine ligand. Both **1a** and **1b** adopt a T-shaped geometry around Pd, as expected for 14-electron ML_3 complexes. The stability of the two structural isomers is similar to each other. **1b** is slightly more stable than **1a**. The conversion from **1a** to **1b** goes through the Y-shaped transition state **TS_3**, overcoming a small barrier of 10.3 kcal/mol. The angles S−Pd−P were calculated to be 97.7° in **1a**, 103.1° in **1b**, and 142.5° in **TS_3**, Figure 5. The feasibility for this three-coordinate mechanism is in agreement with previously reported experimental and theoretical evidence.

Experimentally, it was also found that the thermodynamically more stable *trans*-isomer could also catalyze the cyanothiolation

(17) Braga, A. A. C.; Ujaque, G.; Yano, S.; Maseras, F. *Organometallics* **2006**, *25*, 3647.

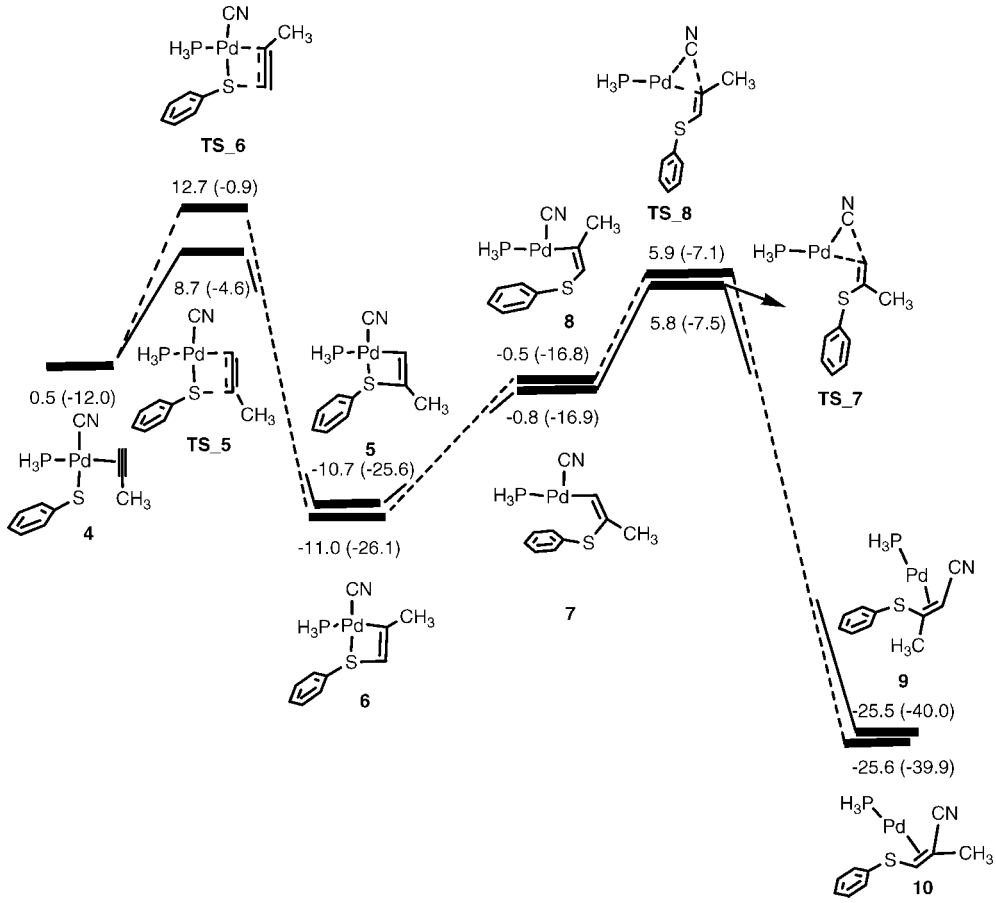

Figure 6. Potential energy profiles calculated for the propyne insertion involving thiopalladation and the reductive elimination steps. The relative free energies and electronic energies (in parentheses) are given in kcal/mol.

of alkynes.[6] Starting from the *trans*-Pd(SPh)(CN)(PH_3)$_2$ complex **3**, substitution of one PH_3 ligand with an 1-alkyne substrate molecule (here propyne as the model substrate) occurs to give **4**, a precursor species ready for insertion reactions (see below). As shown in Figure 4, the ligand substitution is endothermic: **4** + PH_3 is 6.8 kcal/mol less stable than **3** + propyne. The reaction barrier is evaluated to be 20.4 kcal/mol, and the corresponding transition state **TS_4** adopts a typical trigonal-bipyramidal structure with the PhS and CN ligands occupying the two axial sites. The C−C triple-bond distance of the η^2-coordinated propyne was calculated to be 1.228 Å for complex **4**, about 0.02 Å longer than that in the free propyne. In the square-planar complex **4**, the alkyne ligand is perpendicular to the square plane of the complex.

In the catalytic processes, the substitution step may not necessarily occur since the alkyne substrate has a much higher concentration than phosphine and can coordinate to the intermediate **1b** to form complex **4** directly. Even though the *trans*-isomer **3** can be formed much more easily, complex **4** can be obtained via a direct process of **3** → **1b** → **4** without the need of having the substitution step.

C. Propyne Insertion and Reductive Elimination. Starting from **4**, alkyne insertion can occur via either thiopalladation or cyanopalladation. The calculated reaction profiles for the two insertion processes are shown schematically in Figures 6 and 7. Figure 6 is for the thiopalladation process, while Figure 7 is related to the cyanopalladation process. In both the thiopalladation and cyanopalladation processes, each has two possible pathways resulting in different regioselectivity of the alkyne insertion. Comparing the energy profiles depicted in these two figures, we note that although the cyanopalladation generates thermodynamically slightly more stable intermediates **11** and **12**, it must overcome relatively much higher energy barriers than thiopalladation. Therefore, from the energy point of view, the propyne insertion reaction is kinetically determined and goes through thiopalladation.

To probe the reason that the thiopalladation is much more favorable than cyanopalladation, we here examine the HOMO of the complex **4**. As shown in Figure 8, the HOMO is mainly localized at the S atom of the PhS ligand, indicating that in the insertion step the PhS ligand can act as a nucleophile to attack one carbon center of the coordinated alkyne ligand, facilitating the thiopalladation. On the contrary, the cyanopalladation is relatively less likely to occur because the CN ligand contributes little to the HOMO. An NBO charge analysis also shows that the S atom of the PhS ligand in **4** carries a relatively larger negative charge (−0.202) than the C atom of the CN ligand (−0.097). So the S atom could attack the propyne carbon nucleophilically more easily than the C_{CN} atom.

In the two pathways shown for the thiopalladation process (Figure 6), the one involving a 1,2-insertion leading to the formation of the intermediate **5** with the S atom bonded to the substituted carbon atom of propyne has a much lower barrier than the one involving a 2,1-insertion, giving the intermediate **6** with the S atom bonded to the unsubstituted propyne carbon. The two isomeric intermediates **5** and **6** have almost the same stability. The results show that the thiopalladation proceeds via 1,2-insertion preferably, leading to the regioselective products consistent with the experiments. In the subsequent reaction processes illustrated in Figure 6, we note that the two pathways almost have the same energy profiles. All the optimized structures involved in the thiopalladation and cyanopalladation are shown in Figures 9 and 10, respectively. The intermediates **5** and **6** both have a four-membered-ring structure. The Pd−S bond stretches by ca. 0.1 Å in **5** and **6**

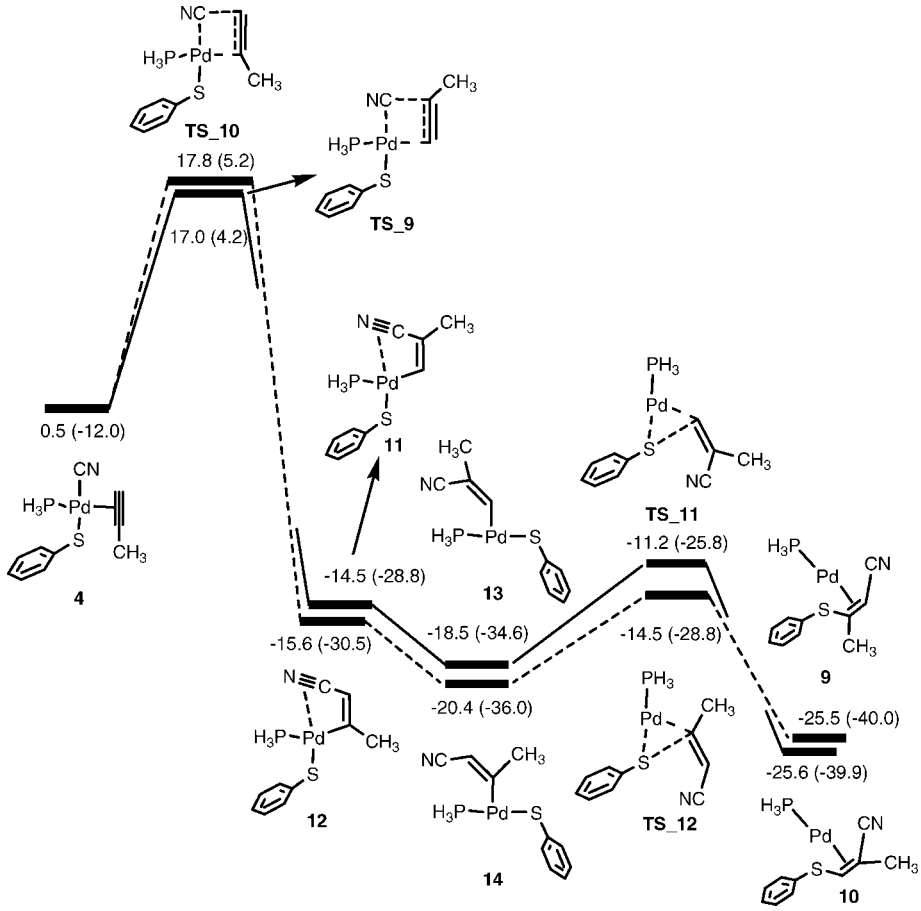

Figure 7. Potential energy profiles calculated for the propyne insertion involving cyanopalladation and the reductive elimination steps. The relative free energies and electronic energies (in parentheses) are given in kcal/mol.

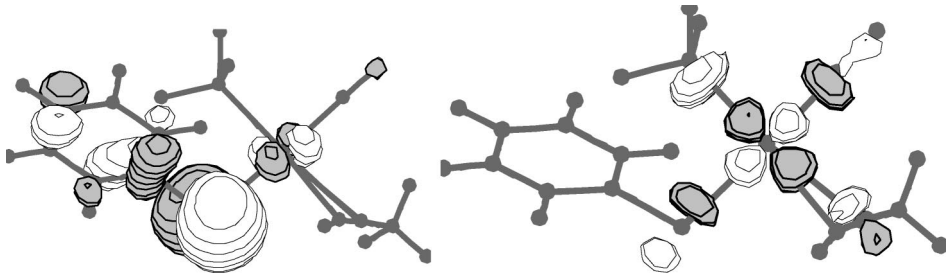

Figure 8. Spatial plots of the HOMO (left) and the LUMO (right) for complex **4**.

compared with that in the π complex **4** and breaks completely in **7** and **8**. In the reductive elimination step the CN ligand migrates to the propyne through the transition states **TS_7** and **TS_8** to form the π complexes **9** and **10**, in which the cyanothiolation product molecule acts as a ligand. The C═C double bond distance in the η^2-coordinated cyanothiolation product molecule was calculated to be 1.404 Å for **9** and 1.407 Å for **10**.

Although complex **4** will not go through cyanopalladation owing to its much higher barrier compared with the thiopalladation, we note from Figure 7 that cyanopalladation has a relatively lower barrier in the subsequent steps, which again have almost the same energy profiles for the two pathways.

D. The Nature of the Insertion of 1-Alkynes into the Pd−S Bond. The alkyne cyanothiolation experiments reported by Ogawa et al. show excellent regioselectivity; that is, the PhS group always attaches to the substituted carbon atom of 1-alkynes eq 1.[6] The results discussed above indicate that the regioselectivity of the reactions are determined by the alkyne insertion step. As shown above, the preference of 1,2-insertion over 2,1-insertion leads to the cyanothiolation products with the PhS group attached to the substituted carbon atom of 1-alkyne.

As mentioned above, the alkyne insertion into the Pd−SPh bond involves a nucleophilic attack of the PhS ligand on the coordinated alkyne in the precursor complex **4**. For the propyne substrate used in the calculations, it is easy to understand the regioselectivity considering that the methyl substituent on propyne is electron-donating, making the unsubstituted carbon more electron rich and making the nucleophilic attack preferentially on the substituted carbon. Indeed, the S atom in the precursor complex **4** carries a large negative charge of −0.202 and the substituted carbon of the propyne ligand carries a positive charge of 0.064. Interestingly, in the experiments phenylacetylene also underwent the same highly regioselective cyanothiolation, although the phenyl substituent is normally considered as electron-withdrawing.

To understand the nature of the insertion of 1-alkynes into the Pd−S bond, we further explored the insertion of other alkynes HC≡CR into the Pd−SPh bond, where R = Ph, CN, and NH_2.

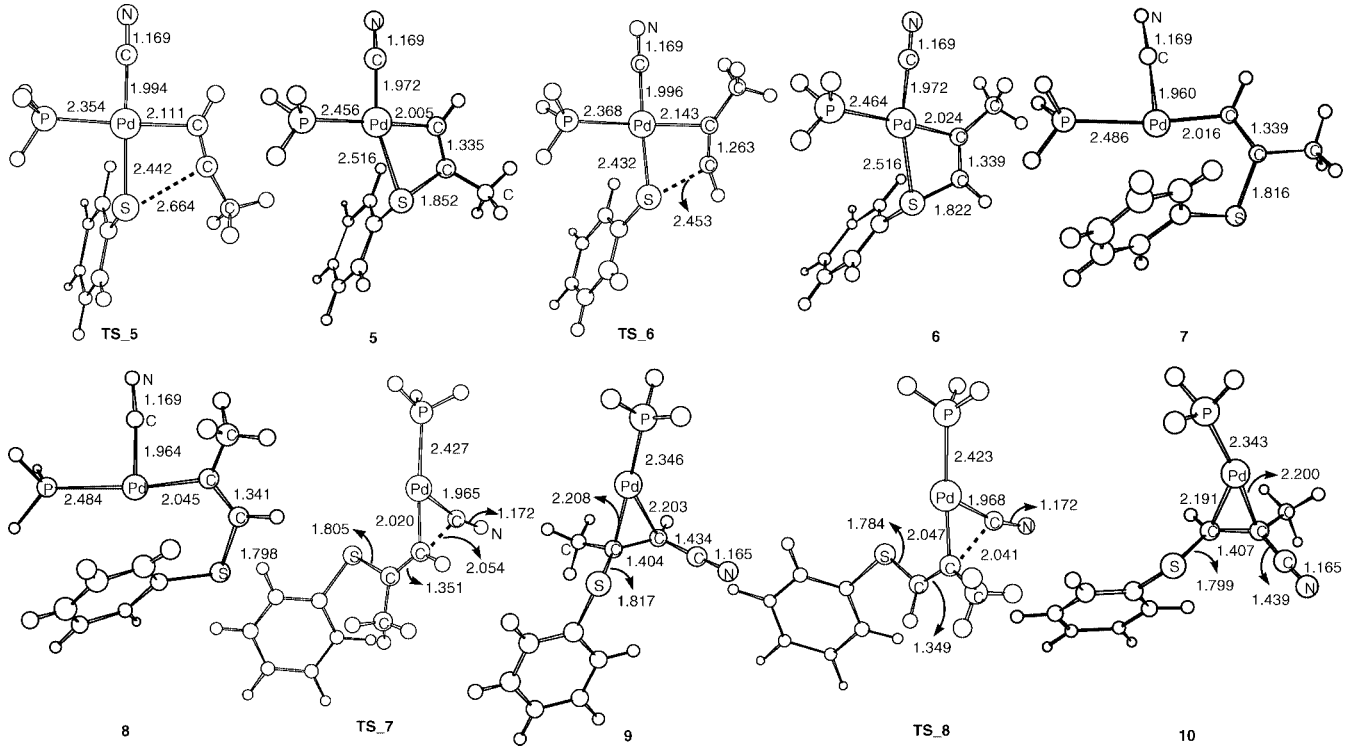

Figure 9. Selected structural parameters (Å) calculated for the species shown in Figure 6.

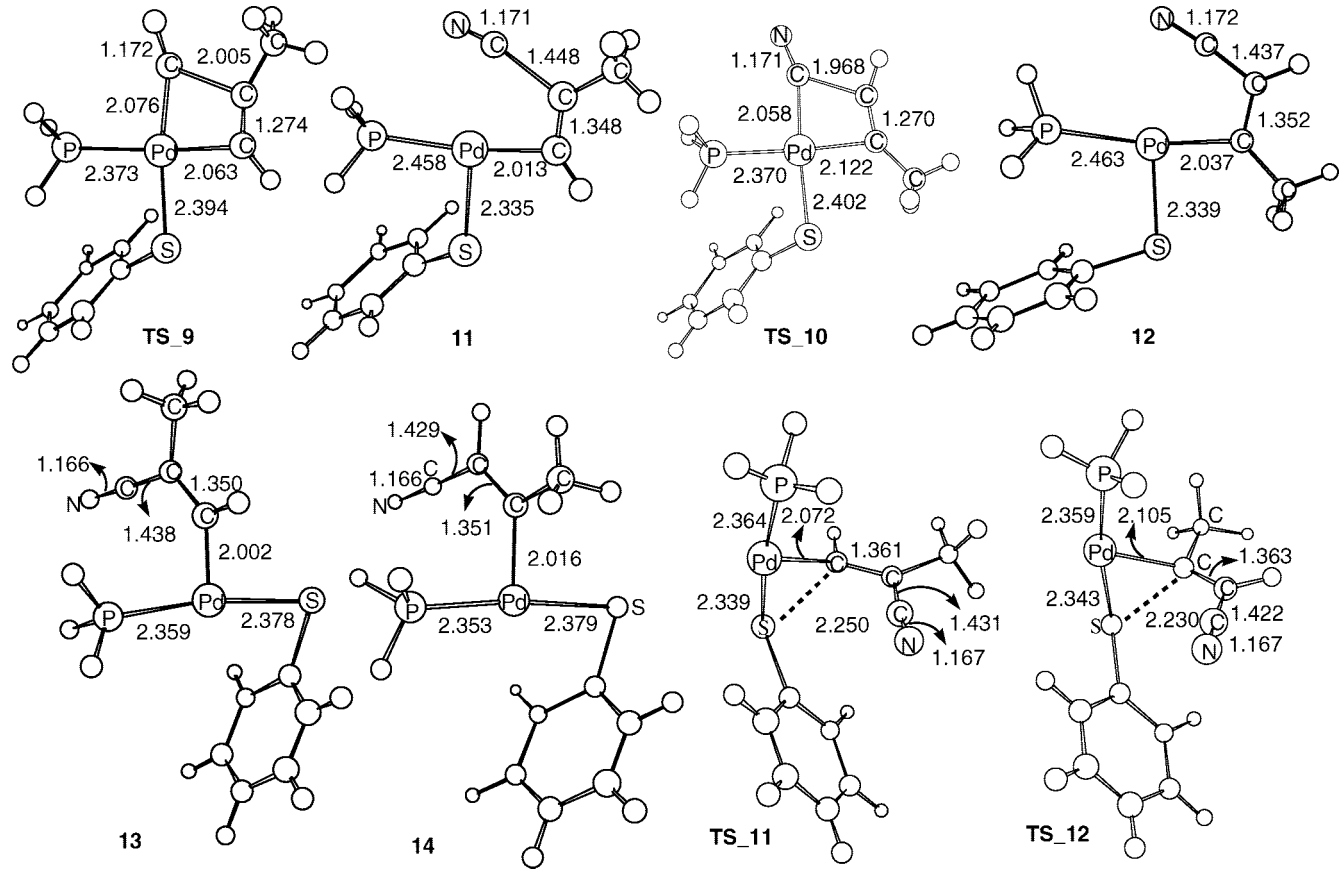

Figure 10. Selected structural parameters (Å) calculated for the species shown in Figure 7.

The calculated energy profiles for these insertion processes are shown in Figure 11. In Figure 11, we used electronic energies for convenience because the entropy contribution is insignificant. An inspection of the results in the figure shows that the 1,2-insertion is kinetically favored in all the cases. Geometrically, the π complexes and the insertion transition states are substantially different, Figure 11. In the π complexes the orientation of the C≡C triple bond is almost perpendicular to the Pd−P−S plane. In the transition states the inserting alkynes almost turn into the square plane around the metal center. This motion is necessary for the

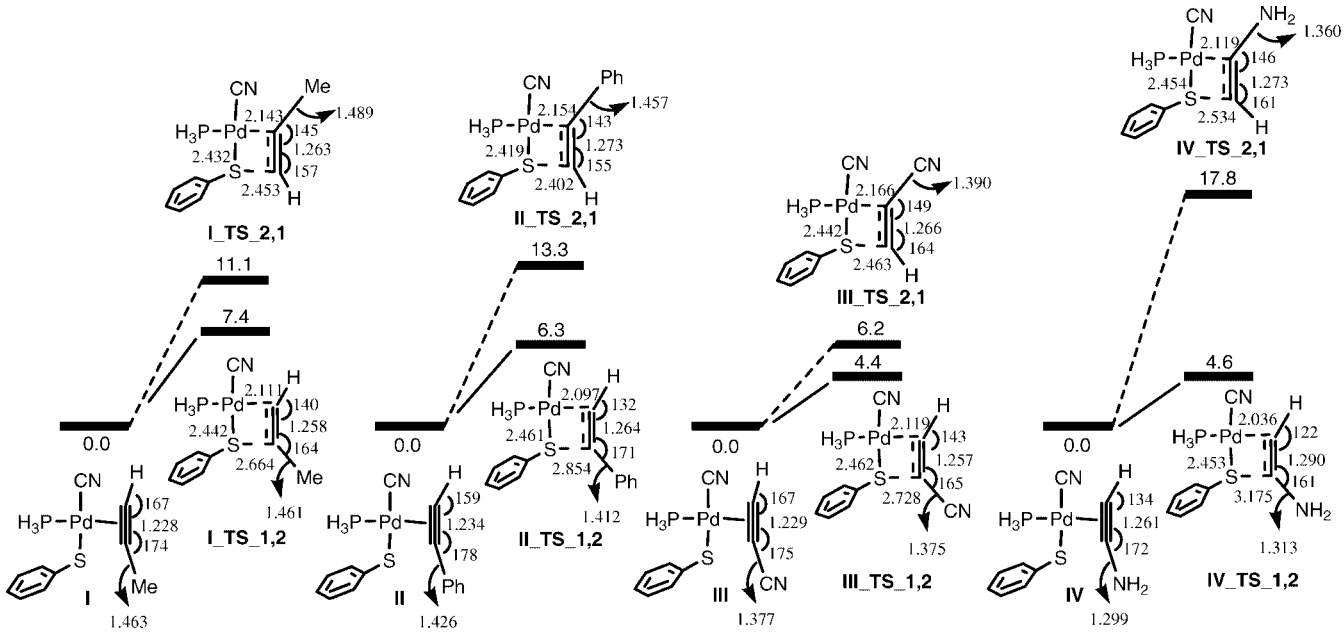

Figure 11. Potential energy profiles and corresponding optimized structures with the geometric parameters calculated for the insertions of 1-alkynes into the Pd−S bond. Bond distances are given in Å, bond angles in deg, and relative electronic energies in kcal/mol.

Scheme 2

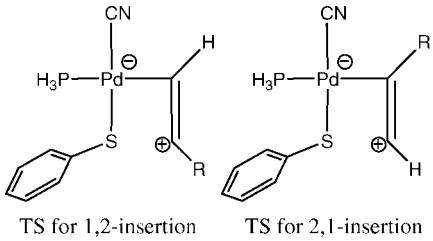

nucleophilic attack of the PhS ligand to the alkyne carbon and provides an early transition state for the insertion, in which the distance between the S atom and the alkyne carbon that forms the C−S bond is still very long and the Pd−S bond elongates only slightly. The structural characteristics in the calculated transition states lead us to believe that the transition states can be described as possessing zwitterionic Lewis structures shown in Scheme 2. In other words, the energy barrier for a given alkyne insertion into the Pd−SPh bond is mainly the energy required to rotate the alkyne ligand into the square plane around the metal center and redistribute the electron density to achieve a zwitterionic Lewis structure like those shown in Scheme 2.

The zwitterionic Lewis structures proposed for the calculated transition structures allow us to explain the regioselectivity results shown in Figure 11. Regardless of whether they are electron-donating or electron-withdrawing, all the substituents studied here (Me, Ph, CN, NH_2) are able to stabilize the TS for 1,2-insertion. Me is known to be able to stabilize a contiguous carbonium center due to its strong electron-donating property. Ph, CN, and NH_2 can stabilize their contiguous carbonium through π-conjugation. π-Conjugation in the transition states can be clearly seen by examining the change in the C−X (X = Me, Ph, CN, NH_2) bond distances from the precursor complexes to the transition states. In the transition state structures for 1,2-insertion, the bond distances are noticeably shortened. In the transition state structures for 2,1-insertion, the bond distances are noticeably lengthened. The HC≡C(CN) substrate shows the smallest preference of 1,2-insertion over 2,1-insertion, while the HC≡C(NH_2) shows the greatest preference, suggesting that the stronger electron-withdrawing property of the CN substituent compromises the π-conjugation effect significantly.

Conclusions

The mechanism of the regioselective cyanothiolation of 1-alkynes with thiocyanates catalyzed by the palladium diphosphine catalyst was theoretically studied with the aid of DFT calculations at the B3LYP level. The calculations show that the cyanothiolation reactions proceed via an oxidative addition of thiocyanates followed by a thiopalladation and then a reductive elimination. In the oxidative addition step the sulfur−cyano (PhS−CN) bond cleavage is kinetically and thermodynamicly more favorable than the carbon−sulfur (Ph−SCN) bond cleavage since the LUMO of the thiocyanates, acting as an acceptor of electrons during the oxidative addition process, corresponds mainly to a π*-antibonding orbital in the SCN moiety, while the unoccupied orbital having the Ph−SCN π*-antibonding character is lying much higher.

The regioselectivities of the reactions are determined in the alkyne insertion step. The calculations on the insertion reactions of various alkynes HC≡CR (R = Me, Ph, CN, and NH_2) into the Pd−SPh bond indicate that the insertion transition states can be described as possessing a zwitterionic Lewis structure in which the carbonium center acts as the SPh receiving center. Therefore, the transition states can be greatly stabilized by substituents capable of π-conjugation with or electron-donation to the contiguous carbonium center in the cases of 1,2-insertion, resulting in the formation of products with the SPh group bonded to the substituted carbon atom of 1-alkynes.

Acknowledgment. We acknowledge financial support from the Hong Kong Research Grants Council (Grant No. HKUST 601507P) A.A. appreciates the financial support from Islamic Azad University, Central Tehran Branch, Iran.

Supporting Information Available: Complete ref 14, Figure S1, and tables giving Cartesian coordinates and electronic energies for all the calculated structures. This material is available free of charge via the Internet at http://pubs.acs.org.

OM7009446